

Fermi level tuning and a large activation gap achieved in the topological insulator $\text{Bi}_2\text{Te}_2\text{Se}$ by Sn doping

Zhi Ren, A. A. Taskin, Satoshi Sasaki, Kouji Segawa, and Yoichi Ando*

Institute of Scientific and Industrial Research, Osaka University, Ibaraki, Osaka 567-0047, Japan

(Dated: March 1, 2013)

We report the effect of Sn doping on the transport properties of the topological insulator $\text{Bi}_2\text{Te}_2\text{Se}$ studied in a series of $\text{Bi}_{2-x}\text{Sn}_x\text{Te}_2\text{Se}$ crystals with $0 \leq x \leq 0.02$. The undoped stoichiometric compound ($x = 0$) shows an n -type metallic behavior with its Fermi level pinned to the conduction band. In the doped compound, it is found that Sn acts as an acceptor and leads to a downshift of the Fermi level. For $x \geq 0.004$, the Fermi level is lowered into the bulk forbidden gap and the crystals present a resistivity considerably larger than $1 \Omega\text{cm}$ at low temperatures. In those crystals, the high-temperature transport properties are essentially governed by thermally-activated carriers whose activation energy is 95–125 meV, which probably signifies the formation of a Sn-related impurity band. In addition, the surface conductance directly obtained from the Shubnikov-de Haas oscillations indicates that a surface-dominated transport can be achieved in samples with several μm thickness.

PACS numbers: 73.25.+i, 74.62.Dh, 72.20.My, 73.20.At

I. INTRODUCTION

In a three-dimensional (3D) topological insulator (TI), a band inversion due to strong spin-orbit coupling induces gapless surface states (SS) consisting of spin helical Dirac Fermions,^{1–5} which are expected to give rise to a number of topological quantum phenomena.^{6,7} Whereas such surface sensitive probes as angle-resolved photoemission spectroscopy (ARPES) and scanning tunneling microscope have been successfully applied to investigate the topological SS,^{8–19} the transport study of the SS remains a challenge due to the presence of parallel bulk conducting channel that usually dominates the transport properties.^{20–28} Recently, the ternary tetradymite $\text{Bi}_2\text{Te}_2\text{Se}$ (BTS) has become a prototype TI material for studying the peculiar spin and charge transport of the SS,^{29,30} because carefully prepared BTS crystals not only present a very low bulk conduction, but also show clear Shubnikov-de Haas (SdH) oscillations that reflect a high mobility of surface Dirac electrons. Given the lack of a truly bulk-insulating state in any of the known TI materials so far,^{31–33} further improvement of BTS is worth pursuing.

The first synthesis of BTS was made while optimizing the continuous solid solutions between Bi_2Te_3 and Bi_2Se_3 for thermoelectric applications.³⁴ Nevertheless, unlike other members in the $\text{Bi}_2\text{Te}_{3-x}\text{Se}_x$ ($0 < x < 3$) family, the Te and Se atoms in BTS occupy distinct crystallographic sites, forming quintuple layers arranged in the sequential order Te-Bi-Se-Bi-Te along the c axis.³⁵ Such chalcogen ordering is believed to provide structural basis for reducing bulk carriers and achieving high surface mobility.²⁹ Unfortunately, similar to Bi_2Se_3 , the BTS crystals grown from the stoichiometric melts show n -type metallic conduction with the electron density n_e of $\sim 10^{19} \text{ cm}^{-3}$.³⁶ When the chalcogen stoichiometry is altered in the starting composition, one obtains^{29,36} metallic or insulating crystals at different positions along the boule,

which is due to the inevitable phase separation during the solidification process, according to a newly established phase diagram of the Bi_2Te_3 – Bi_2Se_3 system.³⁷ Therefore, it is desirable to explore an alternative route to obtain BTS crystals with a large bulk resistivity while keeping the chalcogen stoichiometry, which would be useful for achieving a high surface-carrier mobility.

In this paper, we show that the above objective can be accomplished by hole doping through a Bi-site substitution, which has already been proven to be effective in tuning the carrier type and density for both of the binary end members, Bi_2Te_3 and Bi_2Se_3 .^{10,22,23,28} It is found that, in analogy to its role in Bi_2Te_3 ,^{10,38–40} the group IV element Sn acts as an acceptor in BTS, which allows us to tune the Fermi level (E_F) of this material. In particular, the $\text{Bi}_{2-x}\text{Sn}_x\text{Te}_2\text{Se}$ crystals with $x \geq 0.004$ show low-temperature resistivity reaching several Ωcm , indicating that E_F is tuned into the bulk band gap; their transport properties at high temperatures signify a large activation gap, which probably comes from a Sn-related impurity band. In about a half of those samples, we observed SdH oscillations originating from the topological surface state below 14 T. Our analysis of the SdH oscillations gives direct evidence that one can achieve a surface-dominated transport in a bulk Sn-doped BTS crystal with a thickness of several μm .

II. EXPERIMENTAL DETAILS

The single crystals of $\text{Bi}_{2-x}\text{Sn}_x\text{Te}_2\text{Se}$ were grown by melting high purity elemental shots of Bi (99.9999%), Sn (99.99%), Te (99.9999%), and Se (99.999%) with a nominal ratio of Bi:Sn:Te:Se = $(2-x):x:2:1$ ($x = 0, 0.002, 0.004, 0.006, 0.01, 0.02$) in sealed evacuated quartz tubes at 850°C for 48 h with periodically shaking to ensure homogeneity, followed by cooling slowly to 500°C and then annealing at that temperature for 4 days. The resulting

crystals are easily cleaved along the (111) plane, revealing a shiny mirrorlike surface. The x-ray diffraction (XRD) analysis, which was performed on powders obtained by crushing the crystals, confirmed the samples to be single phase with chalcogen-ordered tetradymite structure.

For transport characterizations, the crystals were cut into bar-shaped samples with the typical thickness of 100 μm after they were checked to be single domain by x-ray Laue analysis. The electrical leads were attached to the samples using room-temperature-cured silver paste in a six-probe configuration. The in-plane resistivity ρ_{xx} and the Hall coefficient R_H were measured in a Quantum Design Physical Properties Measurement System (PPMS-9) down to 1.8 K. The magnetic field was applied along the C_3 axis which is perpendicular to the cleaved surface. For each x value, the data were taken on several crystals obtained from different parts of the boule in order to check for sample-to-sample variation. In addition, selected samples were cleaved down to a few micrometers by using Kapton tapes and then brought to a 14-T magnet for the detection of SdH oscillations using an ac measurement technique, in which two lock-in amplifiers were employed to collect the signals in both the longitudinal (ρ_{xx}) and transverse (ρ_{yx}) channels simultaneously. The measurements were carried out by sweeping the magnetic field between ± 14 T at the rate of 0.3 T/min, during which the temperature was stabilized to within ± 5 mK.

III. RESULTS

A. Resistivity

Figure 1(a) shows typical data for the temperature dependences of ρ_{xx} in $\text{Bi}_{2-x}\text{Sn}_x\text{Te}_2\text{Se}$ crystals with different x values, together with the data for an insulating sample grown from the starting composition $\text{Bi}_2\text{Te}_{1.95}\text{Se}_{1.05}$ which we abbreviate as $\text{BTS}_{1.05}$. The undoped stoichiometric BTS crystal ($x = 0$) shows a metallic behavior in the whole temperature range; correspondingly, the Hall coefficient R_H [inset of Fig. 2(a)] is negative and nearly temperature independent, giving an electron carrier density of $\sim 1.5 \times 10^{19} \text{ cm}^{-3}$ at 1.8 K. This result is in agreement with the previous study,³⁶ which indicated that E_F is pinned to the conduction band for this composition. Upon doping with Sn, a drastic change in both the resistivity value and its temperature dependence was observed. It is worth noting that an insulating behavior of ρ_{xx} is already established even for 0.1% of Sn doping to the Bi site ($x = 0.002$). For $x \geq 0.004$, the ρ_{xx} values reach a few Ωcm , which are usually larger than that achieved in $\text{BTS}_{1.05}$.²⁹

It should be noted that there is a marked difference in the $\rho_{xx}(T)$ behavior between the Sn-doped BTS ($x \geq 0.004$) and the $\text{BTS}_{1.05}$ samples. Firstly, in the high-temperature region, ρ_{xx} in Sn-doped BTS samples increases more steeply with decreasing temperature, as can be seen more clearly in the Arrhenius plot shown in Fig.

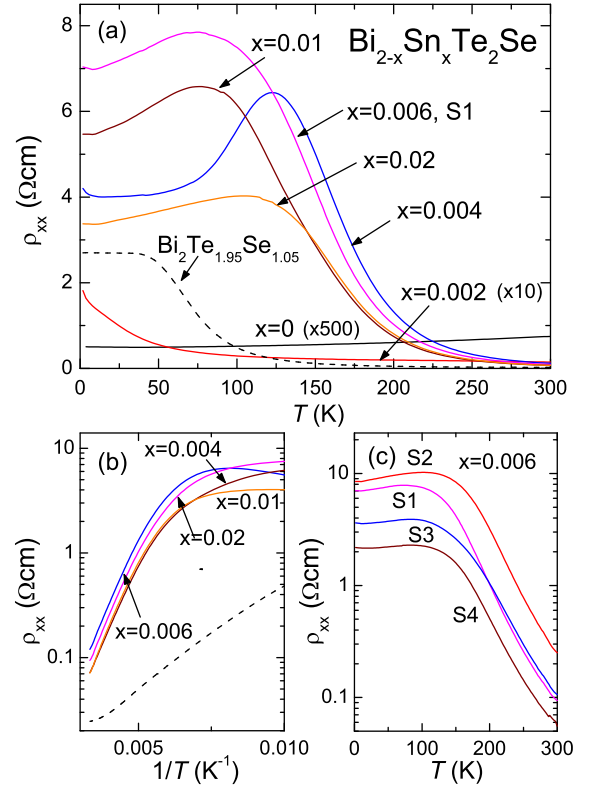


FIG. 1: (Color online) (a) Temperature dependences of ρ_{xx} for $\text{Bi}_{2-x}\text{Sn}_x\text{Te}_2\text{Se}$ single-crystal samples with various x . Note that the data with $x = 0$ and $x = 0.002$ have been magnified by a factor of 500 and 10, respectively. For comparison, the data for an insulating sample grown from the starting composition $\text{Bi}_2\text{Te}_{1.95}\text{Se}_{1.05}$ is also included (dashed line). (b) Arrhenius plot of the $\rho_{xx}(T)$ data for the temperature range between 100 and 300 K. (c) $\rho_{xx}(T)$ data for four representative samples with $x = 0.006$ obtained from different parts of a boule. The data are labeled in numerical order, where S1 and S4 represent first-to-freeze and the end parts, respectively. Note that the vertical axis is in logarithmic scale.

1(b). The magnitude of ρ_{xx} at room temperature in Sn-doped BTS samples varies from 80 to 110 $\text{m}\Omega\text{cm}$, which are considerably larger than that in $\text{BTS}_{1.05}$.²⁹ Also, the high-temperature slope in the Arrhenius plot, which is almost doping independent, corresponds to an activation gap Δ of approximately 120 meV; this is nearly three times larger than that found for the $\text{BTS}_{1.05}$ sample ($\Delta \simeq 45$ meV). Secondly, in the low temperature region, while $\rho_{xx}(T)$ of the $\text{BTS}_{1.05}$ sample becomes nearly flat, the Sn-doped BTS samples show a more strongly temperature-dependent $\rho_{xx}(T)$ behavior with a weak upturn below ~ 10 K, whose origin is not clear at present.

In addition to the above observations, the Sn-doped BTS samples were found to show a higher degree of homogeneity. As an example, Fig. 1(c) shows the $\rho_{xx}(T)$ data for four samples obtained from different parts of a boule for $x = 0.006$. One can see that all the samples show qualitatively similar temperature dependence of ρ_{xx} . Although the ρ_{xx} values still vary between sam-

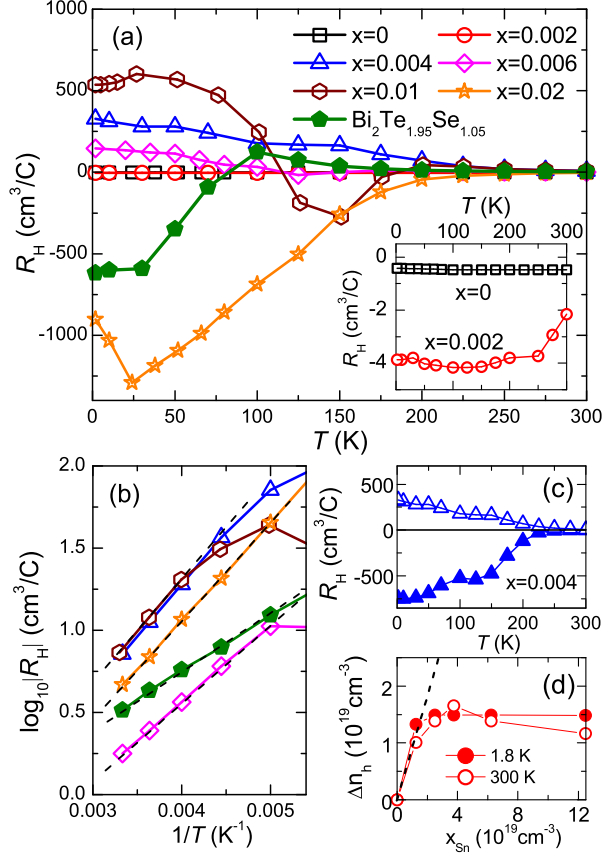


FIG. 2: (Color online) (a) Temperature dependences of the low-field Hall coefficient R_H for a series of $\text{Bi}_{2-x}\text{Sn}_x\text{Te}_2\text{Se}$ samples, together with the data for the $\text{Bi}_2\text{Te}_{1.95}\text{Se}_{1.05}$ sample. The inset shows a magnified view of the data with $x = 0$ and $x = 0.002$. (b) Arrhenius plot of $R_H(T)$ at high temperature for a series of samples except for $x = 0$ and 0.002 where no activation behavior was observed. Dashed lines are the Arrhenius-law fittings to extract the activation energy Δ^* . (c) $R_H(T)$ data for two different samples with $x = 0.004$, showing both n -type and p -type behavior. (d) The density of introduced holes ($\Delta n_h = n(x) - n(0)$) by Sn doping plotted as a function of the density of Sn dopant atoms. The estimation of the carrier density is based on a one-band model for simplicity. The dashed line corresponds to the ideal situation where each Sn atom donates one hole.

ples by a factor of 4, it is notable that all of them are larger than $1\ \Omega\text{cm}$ at low temperature.

B. Hall coefficient

To further investigate the doping effect of Sn in BTS, we measured the Hall resistivity ρ_{yx} . Figure 2(a) shows the temperature dependences of the Hall coefficient R_H for the same series of $\text{Bi}_2\text{Te}_{1.95}\text{Se}_{1.05}$ and $\text{Bi}_{2-x}\text{Sn}_x\text{Te}_2\text{Se}$ samples; here we follow our previous definition of R_H as $R_H = \rho_{yx}/B$ near $B = 0$.³¹ It turns out that 0.1% of Sn doping results in an increase in $|R_H|$ by nearly one order of

magnitude, to $\sim -4\ \text{cm}^3/\text{C}$ at 1.8 K [Fig. 2(a) inset]. Assuming a one-band model, this gives $n_e \simeq 1.6 \times 10^{18}\ \text{cm}^{-3}$, implying that one Sn atom substituted for a Bi atom in BTS introduces approximately one hole, which is much the same as that in the case of n -type Bi_2Te_3 .¹⁰ While R_H is negative for $x = 0$ and 0.002 [Fig. 2(a) inset], it becomes positive at $x = 0.004$ [Fig. 2(a) main panel], suggesting that an n -to- p type transition occurs as a result of Sn doping between $x = 0.002$ and 0.004 . In fact, in the case of $x = 0.004$, both n - and p -type samples with a large $|R_H|$ were found in the same batch [Fig. 2(c)], placing this composition at the verge of such a transition. Somewhat unexpectedly, R_H becomes negative again at a higher doping of $x = 0.02$ [Fig. 2(a)], whose origin is not clear. In the following, we focus on the temperature dependence of R_H for the samples with $x \geq 0.004$.

Above $\sim 200\ \text{K}$, R_H of those samples shows a thermally activated behavior, indicating that E_F is lowered into the bulk band gap. The effective activation gap Δ^* , which is obtained from the Arrhenius plot of $R_H(T)$ shown in Fig. 2(b), is 115, 95, 125, and 110 meV for the samples with $x = 0.004, 0.006, 0.01, 0.02$, respectively. Actually, the Δ^* values for all the measured crystals fall within 95–125 meV for those compositions. These Δ^* values are not far from the Δ values derived from the $\rho_{xx}(T)$ data, and their difference is likely due to the temperature dependence of the carrier mobility. More importantly, the Δ^* values are much larger than that found in the $\text{BiTe}_{1.05}$ sample ($\sim 65\ \text{meV}$), implying that the Sn doping brings E_F closer to the middle of the band gap. At low temperatures, the $|R_H|$ values of those Sn-doped samples become large, sometimes exceeding $1000\ \text{cm}^3/\text{C}$ which would correspond to the carrier density of only $6 \times 10^{15}\ \text{cm}^{-3}$ in a one-band model.

C. Surface quantum oscillations

Although Sn doping is expected to introduce impurity scattering, it turned out that the surface mobility remains reasonably high so that SdH oscillations can still be observed. As a matter of fact, traces of SdH oscillations were detected in nearly 50% of the Sn-doped BTS samples measured in the 14-T magnet. Among those successful cases, the data taken on an n -type sample with $x = 0.004$ (thickness $t = 6\ \mu\text{m}$)⁴¹ showed the simplest pattern of the oscillations. In the following, we present the analysis of this simplest case.

Figure 3(a) shows the magnetic-field dependence of the transverse conductivity G_{yx} of this sample at 1.6 K, which was calculated from ρ_{xx} and ρ_{yx} . SdH oscillations are already visible in the raw data for magnetic field above 10 T. After removing a smooth background, one can clearly see that the oscillatory part of G_{yx} , ΔG_{yx} , exhibits periodic maxima and minima as a function of $1/B$ [Fig. 3(a) inset], establishing the existence of a well defined Fermi surface (FS). In Fig. 3(b), we plot the

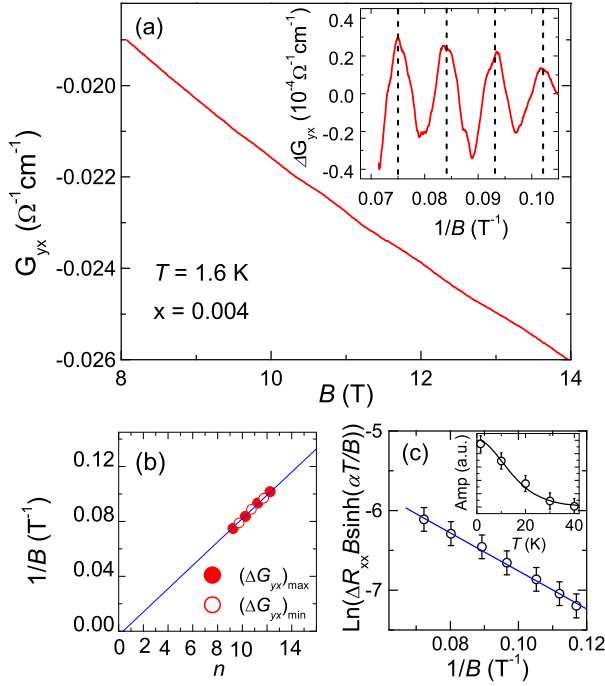


FIG. 3: (Color online) (a) Transverse conductance G_{yx} for an n -type sample with $x = 0.004$ at 1.6 K plotted as a function of magnetic field B applied along the C_3 axis. The inset shows the oscillatory component of G_{yx} , ΔG_{yx} , plotted as a function of $1/B$. The dashed lines are the guide to the eyes. (b) Landau-level fan diagram for oscillations in ΔG_{yx} . Maxima and minima correspond to $n + 1/4$ and $n + 3/4$, respectively. The linear fitting with the slope of $F = 116$ T fixed by the oscillation frequency intersects the axis at $\beta = 0.4 \pm 0.1$. (c) Dingle plot for the oscillations in ΔR_{xx} , yielding $T_D = 12.5$ K; inset shows the temperature dependence of the SdH amplitudes. The solid line represents the fitting by the LK theory, giving $m_c = 0.13m_e$.

$1/B$ values corresponding to the maxima (closed circles) and the minima (open circles) of ΔG_{yx} as a function of the Landau level index n , following the index assignment scheme in Ref. 42. From the linear fitting of the data with the slope fixed at the oscillation frequency obtained from the Fourier transform ($F = 116$ T), we obtain a finite intercept $\beta = 0.4 \pm 0.1$. Since the slope is fixed in this analysis, the error in β is relatively small; the main source of the error is the uncertainty in determining the positions of maxima and minima in the data shown in the inset of Fig. 3(a), and the error of ± 0.1 in β is a conservative estimate. The obtained β of 0.4 ± 0.1 is reasonably close to the value $\beta = 0.5$ expected for massless Dirac Fermions, which points to the topological SS origin of the SdH oscillations. Using the Onsager relation $F = (\hbar c/2\pi e)A$, where A is the extremal FS cross-section area, we find the Fermi wave vector $k_F = 5.9 \times 10^6 \text{ cm}^{-1}$, which corresponds to the surface carrier density $n_s = 2.8 \times 10^{12} \text{ cm}^{-2}$ for a spin-nondegenerate surface state. It is worth noting that if one assumes that the SdH oscillations originate from a bulk FS, the bulk carrier density

implied by F is of the order of 10^{18} cm^{-3} , which is totally inconsistent with the large R_H value observed at 1.8 K ($\sim -100 \text{ cm}^3/\text{C}$). Hence, one can conclude that the SdH oscillations are certainly coming from the surface. From the obtained k_F value and the Fermi velocity $v_F \simeq 4.6 \times 10^5 \text{ m/s}$,²⁹ E_F is estimated to be ~ 170 meV above the Dirac point, pointing to the electron character of the surface carriers.

By fitting the temperature dependence of the oscillation amplitude with the standard Lifshitz-Kosevich (LK) theory [inset of Fig. 3(c)], we obtained the cyclotron mass $m_c = 0.13m_e$, where m_e is the free electron mass. Once m_c is known, the Dingle plot [Fig. 3(c)] gives the Dingle temperature $T_D = 12.5$ K, which corresponds to the surface quantum mobility μ_s^{SdH} of $\sim 1300 \text{ cm}^2/\text{Vs}$. This μ_s^{SdH} value is roughly twice as large as that reported for thick $\text{BTS}_{1.05}$ samples.²⁹ Surprisingly, according to these results, the ratio of the estimated surface conductance to the total conductance, given by G_s/σ , is calculated to be about 1.8 in this sample; here, the surface sheet conductance $G_s = en_s\mu_s^{\text{SdH}} \simeq 5.8 \times 10^{-4} \Omega^{-1}$, the measured overall conductivity σ was $0.64 \Omega^{-1}\text{cm}^{-1}$ at 1.6 K, and $t = 6 \mu\text{m}$.⁴³ Obviously, it is unphysical to have $G_s/\sigma > 1$, and this result implies that the actual surface transport is hindered by steps between terraces created upon cleaving, giving the effective surface conductance that is smaller than the intrinsic one given by n_s and μ_s . Note that a similar problem was reported in Ref. 42. In any case, the SdH oscillations give direct estimate of the surface transport parameters, which indicate that a surface-dominated transport can be achieved in Sn-doped BTS crystals with several μm thickness. The remaining bulk contribution is most likely the degenerate transport through the impurity band which is located in the bulk band gap; to further reduce the bulk contribution, one needs to achieve the Anderson localization in this impurity-band transport.

Apart from this simplest case, the patterns of the observed SdH oscillations were complicated. One of such examples, which was observed in a sample with $x = 0.01$, is shown in Fig. 4. As can be seen in the lower inset, the Fourier transform of $\Delta G_{yx}(B^{-1})$ reveals two well-resolved peaks at $F_1 = 70$ T and $F_2 = 132$ T, reflecting the beating visible in the oscillation data (upper inset). The k_F values calculated from the Onsager relation are 4.6×10^6 and $6.3 \times 10^6 \text{ cm}^{-1}$ for F_1 and F_2 , respectively. These correspond to n_s of 1.7×10^{12} and $3.2 \times 10^{12} \text{ cm}^{-2}$, respectively. Unfortunately, as was pointed out in Ref. 28, the multi-component nature of the oscillations prevents us from reliably extracting the cyclotron mass or the Dingle temperature for each component. Also, the Landau-level fan diagram is not very reliable for extracting β in the multi-component case.

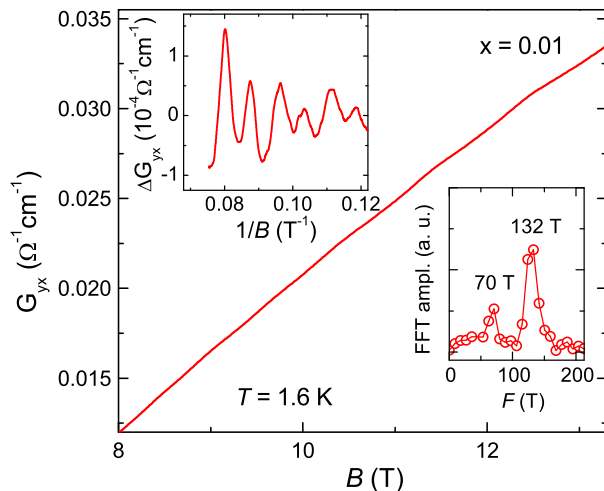


FIG. 4: (Color online) G_{yx} for a sample with $x = 0.01$ at 1.6 K plotted as a function of B applied along the C_3 axis. The upper inset shows the oscillatory component ΔG_{yx} plotted as a function of $1/B$. The lower inset shows the Fourier transform of $\Delta G_{yx}(B^{-1})$, revealing two prominent frequencies.

IV. DISCUSSIONS

From the above results, it is clear that Sn acts as an acceptor in BTS. Ideally, one would expect that the total number of holes introduced by Sn doping, Δn_h , increases linearly with increasing x . However, as can be seen in Fig. 2(d), Δn_h becomes nearly constant for $x \geq 0.004$, which deviates significantly from the ideal situation. Therefore, there must be some additional effects that lead to deactivation of Sn dopants. In this respect, a similar problem was noted in previous studies of Sn doping in Bi_2Te_3 ,^{38–40} and two possibilities have been proposed to explain the apparent discrepancy.

One possibility considered for Bi_2Te_3 is that a part of the Sn atoms are built into the lattice in such a way that a seven-layer lamellar structure, *i.e.* Te-Bi-Te-Sn-Te-Bi-Te, is formed.³⁸ If a similar structure exists in Sn-doped BTS as well, it would be Se-Bi-Te-Sn-Te-Bi-Se. It is important to note that, in contrast to those occupying the Bi site, the Sn atoms in this structure do not bring any charge to the lattice, and thus the discrepancy is reconciled. However, no additional diffraction peaks except for those corresponding to the chalcogen-ordered tetradymite structure were observed in the XRD data even for the sample with the highest Sn-doping concentration (data not shown), suggesting that the seven-layer lamellae, if exist, are randomly distributed in the lattice.

Another, more plausible possibility is that, at high Sn-doping concentration, the wavefunctions of the Sn acceptors overlap significantly, leading to the formation of an impurity band (IB).^{39,40} Within this picture, increasing Sn content results in an increase in the density of states (DOS) of the IB instead of hole doping. In Sn-doped Bi_2Te_3 , this Sn-related IB was shown to be located at 15 meV below the top of the upper valence band.³⁹ However, in the case of Sn-doped BTS, this Sn-related IB is most likely located within the bulk band gap, because the activation energy was found to be much larger in Sn-doped BTS than in $\text{BTS}_{1.05}$, which naturally points to the appearance of a new IB to pin the chemical potential in Sn-doped BTS. Note that, while there may also be IBs due to Se vacancies and Bi/Te antisite defects in Sn-doped BTS, it is most likely that E_F is pinned to the Sn-related IB due to its large DOS. The fact that the activation energy of ~ 120 meV is essentially unchanged for a range of Sn concentrations ($x = 0.004$ – 0.02) is also consistent with this picture. Further studies are called for to clarify the details of the IBs in Sn-doped BTS.

V. CONCLUSION

We performed a systematic study of the transport properties of a series of $\text{Bi}_{2-x}\text{Sn}_x\text{Te}_2\text{Se}$ single crystals with $0 \leq x \leq 0.02$. It is found that Sn behaves as an acceptor, which enables us to tune the Fermi level that is located in the conduction band in the undoped stoichiometric compound. For ≥ 0.004 , E_F is successfully tuned into the bulk band gap, and the resistivity becomes as large as several Ωcm at low temperatures. The transport properties at high temperatures show a thermally activated behavior with a large activation gap, which is probably related to the formation of a Sn-related impurity band. The analysis of the SdH oscillations observed in a $6\text{-}\mu\text{m}$ thick sample indicates that a surface-dominated transport can be achieved in Sn-doped BTS single crystals with several μm thickness. This, along with the large activation gap, makes the Sn-doped BTS system well suited for future applications of topological insulators.

Acknowledgments

This work was supported by JSPS (NEXT Program), MEXT (Innovative Area “Topological Quantum Phenomena” KAKENHI 22103004), and AFOSR (AOARD 104103 and 124038).

* Electronic address: y'ando@sanken.osaka-u.ac.jp

¹ L. Fu, C. L. Kane, and E. J. Mele, Phys. Rev. Lett. **98**, 106803 (2007).

² J.E. Moore and L. Balents, Phys. Rev. B **75**, 121306(R) (2007).

(2007).

³ R. Roy, Phys. Rev. B **79**, 195322 (2009).

⁴ L. Fu and C.L. Kane, Phys. Rev. B **76**, 045302 (2007).

⁵ X-L. Qi, T. L. Hughes, and S.-C. Zhang, Phys. Rev. B **78**,

- 195424 (2008).
- ⁶ M.Z. Hasan and C.L. Kane, *Rev. Mod. Phys.* **82**, 3045 (2010).
 - ⁷ X.L. Qi and S.C. Zhang, *Rev. Mod. Phys.* **83**, 1057 (2010).
 - ⁸ D. Hsieh, D. Qian, L. Wray, Y. Xia, Y.S. Hor, R.J. Cava, and M.Z. Hasan, *Nature* **452**, 970 (2008).
 - ⁹ A. Nishide, A.A. Taskin, Y. Takeichi, T. Okuda, A. Kakizaki, T. Hirahara, K. Nakatsuji, F. Komori, Y. Ando, and I. Matsuda, *Phys. Rev. B* **81**, 041309(R) (2010).
 - ¹⁰ Y.L. Chen, J.G. Analytis, J.-H. Chu, Z.K. Liu, S.-K. Mo, X.L. Qi, H.J. Zhang, D.H. Lu, X. Dai, Z. Fang, S.C. Zhang, I.R. Fisher, Z. Hussain, and Z.-X. Shen, *Science* **325**, 178 (2009).
 - ¹¹ T. Sato, K. Segawa, H. Guo, K. Sugawara, S. Souma, T. Takahashi, and Y. Ando, *Phys. Rev. Lett.* **105**, 136802 (2010).
 - ¹² K. Kuroda, M. Ye, A. Kimura, S.V. Ereemeev, E.E. Krasovskii, E.V. Chulkov, Y. Ueda, K. Miyamoto, T. Okuda, K. Shimada, H. Namatame, and M. Taniguchi, *Phys. Rev. Lett.* **105**, 146801 (2010).
 - ¹³ Y.L. Chen, Z.K. Liu, J.G. Analytis, J.-H. Chu, H.J. Zhang, B.H. Yan, S.-K. Mo, R.G. Moore, D.H. Lu, I.R. Fisher, S.-C. Zhang, Z. Hussain, and Z.-X. Shen, *Phys. Rev. Lett.* **105**, 266401 (2010).
 - ¹⁴ S.Y. Xu, L.A. Wray, Y. Xia, R. Shankar, A. Petersen, A. Fedorov, H. Lin, A. Bansil, Y.S. Hor, D. Grauer, R.J. Cava, and M.Z. Hasan, *arXiv:1007.5111v1*.
 - ¹⁵ T. Arakane, T. Sato, S. Souma, K. Kosaka, K. Nakayama, M. Komatsu, T. Takahashi, Z. Ren, K. Segawa, and Y. Ando, *Nat. Commun.* **3**, 636 (2012).
 - ¹⁶ P. Roushan, J. Seo, C.V. Parker, Y.S. Hor, D. Hsieh, D. Qian, A. Richardella, M.Z. Hasan, R.J. Cava, and A. Yazdani, *Nature* **460**, 1106 (2009).
 - ¹⁷ Z. Alpichshev, J.G. Analytis, J.H. Chu, I.R. Fisher, Y.L. Chen, Z.X. Shen, A. Fang, and A. Kapitulnik, *Phys. Rev. Lett.* **104**, 016401 (2010).
 - ¹⁸ P. Cheng, C.L. Song, T. Zhang, Y.Y. Zhang, Y.L. Wang, J.F. Jia, J. Wang, Y.Y. Wang, B.F. Zhu, X. Chen, X.C. Ma, K. He, L.L. Wang, X. Dai, Z. Fang, X.C. Xie, X.L. Qi, C.X. Liu, S.C. Zhang, and Q.K. Xue, *Phys. Rev. Lett.* **105**, 076801 (2010).
 - ¹⁹ T. Hanaguri, K. Igarashi, M. Kawamura, H. Takagi, and T. Sasagawa, *Phys. Rev. B* **82**, 081305(R) (2010).
 - ²⁰ A.A. Taskin and Y. Ando, *Phys. Rev. B* **80**, 085303 (2009).
 - ²¹ D.-X. Qu, Y.S. Hor, J. Xiong, R.J. Cava, and N.P. Ong, *Science* **329**, 821 (2010).
 - ²² J.G. Analytis, R.D. McDonald, S.C. Riggs, J.-H. Chu, G.S. Boebinger, and I.R. Fisher, *Nat. Phys.* **10**, 960-964 (2010).
 - ²³ Y.S. Hor, A. Richardella, P. Roushan, Y. Xia, J.G. Checkelsky, A. Yazdani, M.Z. Hasan, N.P. Ong, and R.J. Cava, *Phys. Rev. B* **79**, 195208 (2009).
 - ²⁴ J.G. Checkelsky, Y.S. Hor, M.-H. Liu, D.-X. Qu, R.J. Cava, and N.P. Ong, *Phys. Rev. Lett.* **103**, 246601 (2009).
 - ²⁵ N.P. Butch, K. Kirshenbaum, P. Syers, A.B. Sushkov, G.S. Jenkins, H.D. Drew, and J. Paglione, *Phys. Rev. B* **81**, 241301 (2010).
 - ²⁶ J.G. Analytis, J.H. Chu, Y. Chen, F. Corredor, R.D. McDonald, Z.X. Shen, and I.R. Fisher, *Phys. Rev. B* **81**, 205407 (2010).
 - ²⁷ K. Eto, Z. Ren, A.A. Taskin, K. Segawa, and Y. Ando, *Phys. Rev. B* **81**, 195309 (2010).
 - ²⁸ Z. Ren, A.A. Taskin, S. Sasaki, K. Segawa, and Y. Ando, *Phys. Rev. B* **84**, 075316 (2011).
 - ²⁹ Z. Ren, A.A. Taskin, S. Sasaki, K. Segawa, and Y. Ando, *Phys. Rev. B* **82**, 241306(R) (2010).
 - ³⁰ J. Xiong, A.C. Petersen, D.X. Qu, R.J. Cava, and N.P. Ong, *arXiv:1101.1315*.
 - ³¹ Z. Ren, A.A. Taskin, S. Sasaki, K. Segawa, and Y. Ando, *Phys. Rev. B* **84**, 165311 (2011).
 - ³² A.A. Taskin, Z. Ren, S. Sasaki, K. Segawa, and Y. Ando, *Phys. Rev. Lett.* **107**, 016801 (2011).
 - ³³ C. Brune, C. X. Liu, E. G. Novik, E. M. Hankiewicz, H. Buhmann, Y. L. Chen, X. L. Qi, Z. X. Shen, S. C. Zhang, and L. W. Molenkamp, *Phys. Rev. Lett.* **106**, 126803 (2011).
 - ³⁴ N. Fuschillo, J.N. Bierly, and F.J. Donahoe, *J. Phys. Chem. Solids* **8**, 430 (1959).
 - ³⁵ S. Nakajima, *J. Phys. Chem. Solids* **24**, 479 (1963).
 - ³⁶ S. Jia, H.W. Ji, E. Climent-Pascual, M.K. Fuccillo, M.E. Charles, J. Xiong, N.P. Ong, and R.J. Cava, *Phys. Rev. B* **84**, 235206 (2011).
 - ³⁷ O.B. Sokolov, S. Ya. Skipidarov, N.I. Duvankov, and G.G. Shabunina, *J. Cryst. Growth* **262**, 442 (2004).
 - ³⁸ J. Horák, P. Lošták, and J. Guerts, *Phys. Stat. Sol. (b)* **167**, 459 (1991).
 - ³⁹ V.A. Kulbachinskii, M. Inoue, M. Sasaki, H. Negishi, W.X. Gao, K. Takase, Y. Giman, P. Lostak, and J. Horak, *Phys. Rev. B* **50**, 16921 (1994).
 - ⁴⁰ C.M. Jaworski, V. Kulbachinskii, and J.P. Heremans, *Phys. Rev. B* **80**, 233201 (2009).
 - ⁴¹ In $\text{Bi}_{1.5}\text{Sb}_{0.5}\text{Te}_{1.7}\text{Se}_{1.3}$ samples with the thickness of several μm , we observed³² that the low-temperature R_H undergoes a sign change with time and that the SdH frequency accordingly shows a drastic change. However, for the present sample, only a slight time evolution in R_H and the SdH frequency was observed.
 - ⁴² J. Xiong, Y.K. Luo, Y.H. Koo, S. Jia, R.J. Cava, and N.P. Ong, *arXiv:1111.6031*.
 - ⁴³ It should be noted that in the present experiment, the bottom surface of the sample was glued to a Kapton tape, so the top and bottom surfaces were in different environments. This means that the surface chemical potentials (and hence the surface carrier densities) for the top and bottom surfaces were most likely different; nevertheless, only a single frequency was observed in the SdH oscillations, suggesting that only one surface was responsible for the oscillations. We therefore considered only one surface in this calculation of G_s .